Ultrafast demagnetization dynamics in the epitaxial FeGe(111) film chiral magnet

Zizhao Gong,[1,2,*] Wei Zhang,[1,2,*] Jianan Liu,[1,2] Zongkai Xie,[1,2] Xu Yang,[1,2,3] Jin Tang,[4] Haifeng Du,[4,5] Na Li,[1,2] Xiangqun Zhang,[1] Wei He,[1] and Zhao-hua Cheng[1,2,3,†]

[1]*State Key Laboratory of Magnetism and Beijing National Laboratory for Condensed Matter Physics, Institute of Physics, Chinese Academy of Sciences, Beijing 100190, China*

[2]*School of Physical Sciences, University of Chinese Academy of Sciences, Beijing 100049, China*

[3]*Songshan Lake Materials Laboratory, Dongguan, Guangdong 523808, China*

[4]*Anhui Province Key Laboratory of Condensed Matter Physics at Extreme Conditions, High Magnetic Field Laboratory, HFIPS, Anhui, Chinese Academy of Sciences, Hefei, 230031, China*

[5]*Institutes of Physical Science and Information Technology, Anhui University, Hefei 230601, China*

(Received 12 April 2022; accepted 11 April 2023; published 25 April 2023)

The exploring of ultrafast demagnetization is a significant subject for understanding the versatility of spin dynamics. However, the laser-induced ultrafast demagnetization process in chiral magnet FeGe has remained elusive. Here, we report the ultrafast demagnetization processes of FeGe film with various magnetic structures using time-resolved magneto-optical Kerr effect (TRMOKE) measurements. Our work reveals a transition from one-step ultrafast demagnetization (type I) to two-step demagnetization (type II) process by changing ambient temperature, laser fluence, and magnetic field. We confirm that the transition from one-step to two-step ultrafast demagnetization mainly results from the weak electron-phonon (*e-p*) coupling. In the skyrmion phase region, TRMOKE curves demonstrate a two-step ultrafast demagnetization process. The two-step ultrafast demagnetization will further enhance the magnetization loss, and consequently facilitate the magnetization switching and pave a pathway to engineer chiral magnetic devices on picosecond timescales.

DOI: 10.1103/PhysRevB.107.144429

I. INTRODUCTION

Ultrafast demagnetization has attracted much attention for its potential applications in ultrafast information technology and intriguing physics [1–5]. The manipulation of topologically nontrivial phases [6] by optical excitation [7–10] is also an emerging area of condensed-matter physics. Moreover, controlling the timescale and amplitude of the response of spins to a femtosecond laser excitation is a key issue in the fields of magnetic recording [11], ultrafast spintronic devices [12], and magnonics [13]. Chiral magnets are incredible materials in which exotic skyrmion spin textures exist stably favored by the Dzyaloshinskii-Moriya interaction (DMI) [14–18]. Although optically driven collective spin excitations and dynamics modes [19] have been investigated in some chiral magnets, the ultrafast demagnetization process, which is of great significance to control spins on subpicosecond timescale, has not been investigated yet. Previous time-dependent density-functional theory calculation demonstrated that the initial spin disorder played a dominant role and enhanced the demagnetization [20], while the effect of spin texture on ultrafast demagnetization process was rarely reported [4]. The investigation of ultrafast demagnetization in chiral magnets can help understanding the versatility of ultrafast spin dynamics and pave a pathway for the optical manipulation of their magnetic orders.

Chiral magnets with B20 crystal structure are typical skyrmion-hosting materials, such as MnSi [14], $Fe_{1-x}Co_xSi$ [16], and FeGe [15,21,22]. Among them, FeGe possesses the highest Curie temperature of $T_c = 278$ K. Compared with corresponding bulk material, a robust magnetic skyrmion phase in epitaxial FeGe(111) thin films is formed in wider temperature and magnetic field range [23], and consequently provide a platform to investigate the ultrafast demagnetization processes of different magnetic phases. Recently, ultrashort laser pulses were proved to offer a fast and energy-efficient means to create, erase, and manipulate skyrmions [8]. It is highly desirable to explore the laser-induced ultrafast demagnetization process in chiral magnet FeGe film with various magnetic structures.

In this work, we report ultrafast time-resolved magneto-optical Kerr effect (TRMOKE) measurements and find a transition from one-step ultrafast demagnetization process to two-step one in FeGe thin film by altering temperature, magnetic field, as well as laser fluence. Based on the microscopic three-temperature model (M3TM) and time-resolved reflectivity results, we confirm that the transition from one-step to two-step ultrafast demagnetization mainly results from the weak electron-phonon (*e-p*) coupling. Although a similar transition from type-I ultrafast demagnetization process to type-II one was observed in Ni thin film by altering temperature and laser fluence, there are three distinct features between our results and previous works [2,24]. (1) Our results demonstrate

*These authors contributed equally to this work.
†Corresponding author: zhcheng@iphy.ac.cn

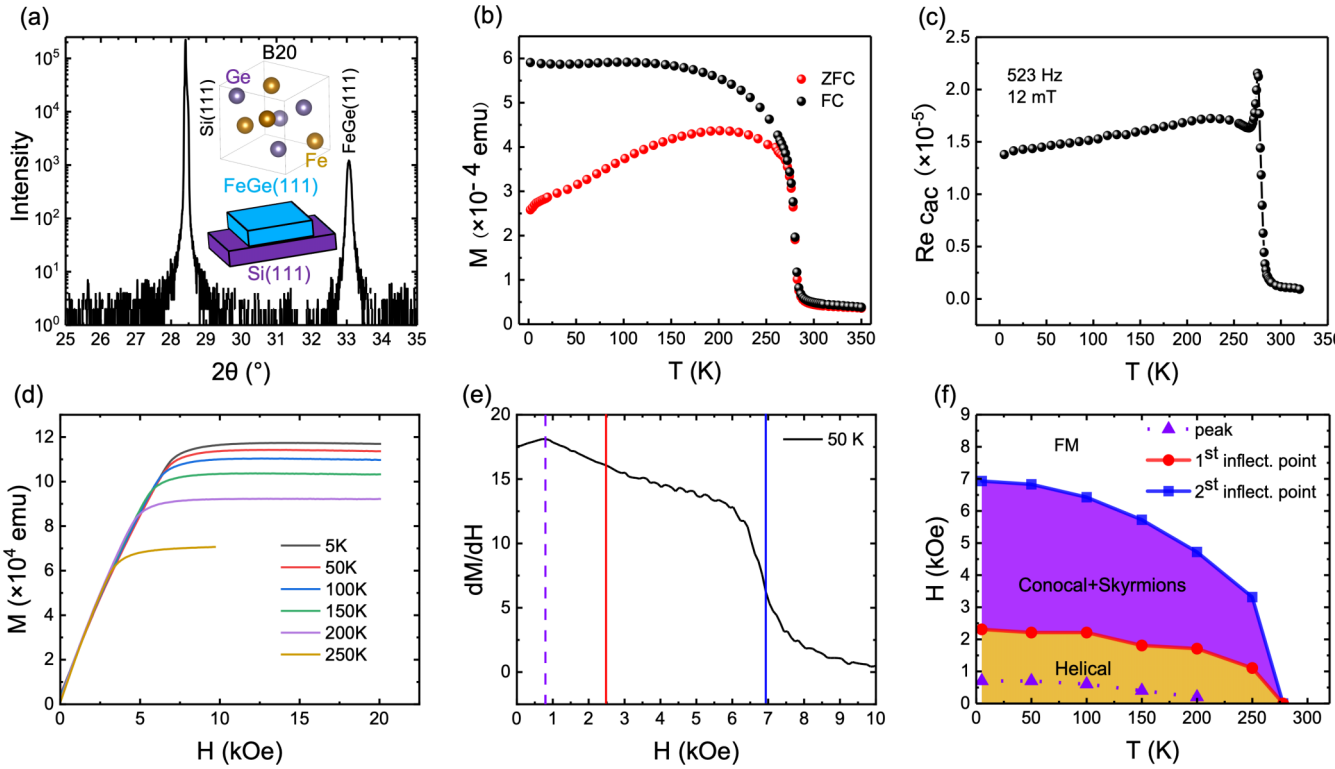

FIG. 1. Structure and magnetism of FeGe film. (a) XRD pattern of the FeGe thin film. Insets represent the configuration of FeGe/Si(111) film and unit cell of B20 FeGe; (b), (c) the in-plane *M-T* curves and ac susceptibility; and (d) field dependence of out-of-plane magnetization at different temperatures. Magnetic phase diagram (f) was derived from the peak and inflection points of *dM/dH* curves in (e).

that for FeGe film the transition undergoes in a broader temperature range and relatively lower laser fluence. (2) In our FeGe film, the mechanism for the two-step demagnetization is different from that in previous works on Ni and other ferromagnetic or antiferromagnetic materials. In the previous work, as mentioned in Refs. [2,24], type-I demagnetization is generally expected to occur when coupling between the electron and spin system is strong, whereas type-II demagnetization is present when the electron-spin (*e-s*) coupling is weak. However, in chiral magnet FeGe film, we have found that the two-step demagnetization mainly originates from weak *e-p* coupling. (3) The M3TM provides a framework to discuss the ultrafast demagnetization in temperature and laser fluence scenario previously, while our results also reveal the magnetic field/phase-dependence demagnetization behavior. We also find that in the skyrmion phase region TRMOKE curves demonstrate a two-step ultrafast demagnetization process. The two-step demagnetization will facilitate to switch magnetization of FeGe films and utilize chiral magnetic devices on picosecond timescales.

II. EXPERIMENT DETAILS

A. Sample preparation

FeGe film was deposited on Si(111) substrate by ultrahigh-vacuum (UHV) molecular-beam epitaxy with a base pressure of 3×10^{-10} mbar. Before the film growth, high-resistance Si(111) substrate was heated to 300 °C for about 8 h and then flashed to 1200 °C to get 7×7 surface in the UHV chamber. Fe and Ge were coevaporated at the same rate onto the Si(111)$-(7 \times 7)$ surface at 300 °C and the deposition rate of FeGe is 0.95 nm/min.

B. Magnetization measurements

The magnetization measurements were performed by a superconducting quantum interference device magnetometer. For the in-plane magnetization, *M-T* curves and ac susceptibility were measured. For the temperature dependence of magnetization, we employed both zero-field-cooled and field-cooled protocol to the desired temperature. The ac susceptibility was measured at an ac field with excitation amplitude of 12 Oe and excitation frequency of 523 Hz. For out-of-plane magnetization, we measured the field dependence of magnetization with zero-field-cooled protocol ramping from $H = 0$ to 20 kOe at 5, 50, 100, 150, 200, and 250 K. Figure 1(e) represents the susceptibility $\chi = dM/dH$ as a function of H at 50 K. The inflection points as marked in Fig. 1(f) with solid lines indicate phase boundaries, and the peak at low field is believed to be related to helical reorientation in the film [25].

C. TRMOKE experiments

The ultrafast demagnetization curves of FeGe were measured by TRMOKE method from 10 to 300 K using pump-probe technique. In the experimental setup, the ultrafast laser with 55-fs pulse width at a 5.2-MHz repetition rate was used. The wavelength of the pump pulses was 780 nm, while the probe pulses were frequency doubled by a beta barium

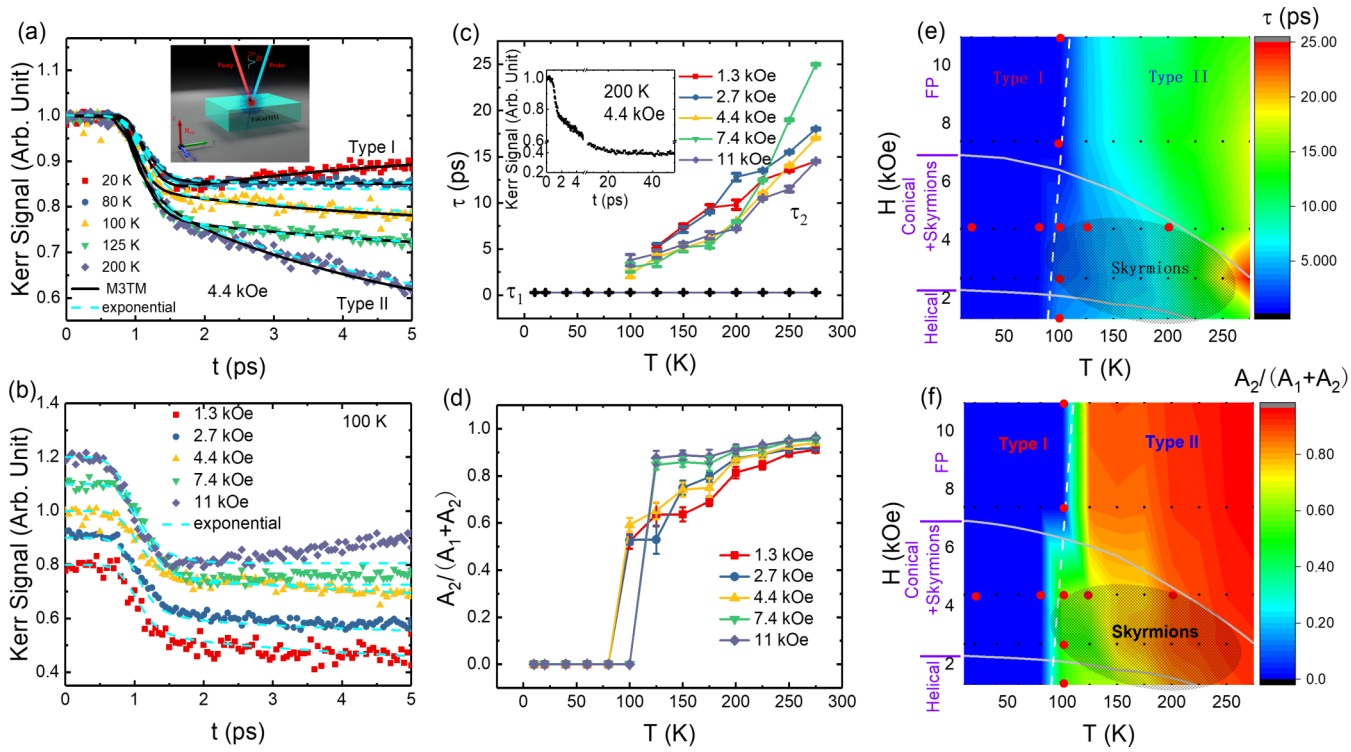

FIG. 2. TRMOKE results. (a), (b) Dependence of the ultrafast demagnetization of FeGe film on the ambient temperature scenario and field scenario. Cyan dashed lines are exponential fittings. Curves in (b) are shifted to avoid the overlap. Inset shows the schematic of TRMOKE measurement. (c), (d) Demagnetization times and amplitude ratios between the second and first step obtained by biexponential function. Inset in (c) is a example curve shown up to 50 ps. (e), (f) Magnetic phase diagrams of FeGe obtained by magnetization measurements. Gray solid lines are the boundaries of magnetic phases. Elliptic shadow is a reference skyrmion region. Color map in (e) and (f) represents the data in (c) and (d), respectively. The white dashed line is the boundary between type-I and type-II demagnetization. Black dots are all the TRMOKE measurement points; red dots are the data points shown in (a) and (b).

borate crystal. In the magnetization dynamics measurements, three external factors, ambient temperature, external magnetic field, and the fluence F of the pumping pulses, were taken into consideration. For the ambient temperature and magnetic field scenario, the fluence F was kept at a constant of $0.7\,\mathrm{mJ/cm^2}$.

III. RESULTS

A. Structural and magnetic characterization

FeGe film with thickness of 140 nm was used in our experiments. The x-ray-diffraction (XRD) pattern [Fig. 1(a)] indicates that the FeGe film is pure B20 phase with (111) orientation.

Figures 1(b) and 1(c) show the temperature dependence of in-plane magnetization and ac susceptibility for epitaxial FeGe(111) thin film, respectively. One can obtain the Curie temperature of $T_c \approx 278$ K, which is the same as that of FeGe bulk crystals [26,27]. The ac susceptibility exhibits a kinklike feature near the Curie temperature, implying that the A phase [14,23,28] exists in this region. The out-of-plane magnetization is shown in Fig. 1(d) and consistent with that of FeGe thin films in previous studies [25]. Based on the methodology established by Bauer *et al.* [28], we performed magnetization measurements as a function of magnetic field and temperature. The magnetic diagram [Fig. 1(f)] of FeGe/Si(111) thin film was determined by the inflection points of the susceptibility $\chi = dM/dH$ vs H [Fig. 1(e)]. We assign the three phases as "helical" for low fields, "conical+skyrmions" for intermediate fields, and "field polarized (FP)" for high fields. The magnetic phase boundaries are consistent with those previously reported for FeGe films [23,25,29].

B. TRMOKE measurements

We employed TRMOKE spectroscopy to probe the ultrafast demagnetization in the whole magnetic phase diagram of FeGe film with polar configuration [inset of Fig. 2(a)]. The dependence of the ultrafast demagnetization of FeGe film on ambient temperature in a magnetic field of 4.4 kOe is shown in Fig. 2(a). In the case of one-step ultrafast demagnetization, i.e., type I, a rapid decrease with the ultrafast demagnetization time is followed by magnetization recovery. Mathematically, the slope changes sign at the inflection point. On the other hand, in the case of two-step demagnetization process, i.e., type II, a slow demagnetization follows the first step; the sign of slope does not change. The critical point of about 100 K can be obtained on the basis of the slope of temperature-dependent demagnetization curves. At temperatures below 100 K, the curves demonstrate one-step demagnetization (type I) with the ultrafast demagnetization time about $\tau_1 \approx 300$ fs, followed by magnetization recovery. With increasing the ambient temperature above 100 K, a transition from one-step (type-I) to two-step (type-II) ultrafast demagnetization process, i.e., a slow demagnetization with time constant

$\tau_2 \approx 3-17$ ps following the first step, occurs. Figure 2(b) shows the ultrafast demagnetization curves in various magnetic fields at $T = 100$ K. At this temperature, type-II demagnetization dynamics becomes dominant when $H < 7.4$ kOe. With further increasing the magnetic field up to 11.0 kOe, the ultrafast demagnetization shows a type-I behavior. From all the demagnetization curves, we can clearly see the magnetization loss of type II is much higher than that of type I. (In the paper, we did not calibrate the measured curves to real demagnetization. All comparisons are based on relative values.) This implies that the second-step ultrafast demagnetization will further enhance the magnetization loss, and consequently facilitate the magnetization switching of FeGe films and may be utilized in high-speed chiral magnetic devices.

It is known that the most essential characteristics of ultrafast demagnetization are demagnetization time and amplitude [2,20]. To investigate two-step ultrafast demagnetization time and magnetization loss of FeGe film quantitatively, an inspection of the measured two-step ultrafast demagnetization by the biexponential function was performed to achieve the timescales of the demagnetization:

$$M(t) = G(t)\left(y_0 - A_1 \times \left(1 - \exp\left(-\frac{t}{\tau_1}\right)\right) - A_2 \times \left(1 - \exp\left(-\frac{t}{\tau_2}\right)\right)\right), \quad (1)$$

where the pulse signal $G(t)$ is convolved into the function. τ_1 and τ_2 are timescales corresponding to the fast and slow demagnetization processes, respectively. A_1 and A_2 represent the amplitudes of the two demagnetization steps, respectively. Since the MOKE signal is proportional to the magnetization, it is not necessary to calibrate the real demagnetization for the same sample. During the TRMOKE measurements, we keep the intensity of incident light invariable, and obtain TRMOKE signals. The ratio of $A_2/(A_1 + A_2)$ is the same as the ratio of real demagnetization.

It should be mentioned that Eq. (1) only considers quenching of magnetization and does not consider recovery of magnetization. Based on the mathematical formation of Eq. (1), the demagnetization can be seen as superposition of two exponential curves with different timescale. For the type-I demagnetization curve, $A_2 = 0$. Figures 2(c) and 2(d) represent the temperature dependence of the demagnetization time (τ_1 and τ_2) and amplitude ratio of the second-step magnetic loss to the total one $A_2/(A_1 + A_2)$ with various applied magnetic fields, respectively. τ_1 is 0.30 ± 0.01 ps and keeps constant when ambient temperature and applied magnetic field change, whereas the second-step demagnetization time increases from 3.00 ± 0.50 ps to 25.00 ± 0.10 ps. Once type-II ultrafast demagnetization process occurs, the second-step demagnetization exceeds 50% of the total demagnetization, and the proportion increases with temperature. As shown in Figs. 2(e) and 2(f), we mapped these two parameters on the magnetic phase diagram. In Fig. 2(e) we use the total demagnetization time $\tau = \tau_1 + \tau_2$ to represent the demagnetization behavior. The diagram is divided into type-I and type-II regions by a white dashed line. According to the results of real-space observation [15] and topological Hall effect [23], we mark the reference skyrmion phase region with shadows in Figs. 2(e) and 2(f). One can find that in the skyrmion phase region TRMOKE curves show a two-step ultrafast demagnetization process. The phase boundaries of helical, conical+skyrmions, and field polarized are shown in Figs. 2(e) and 2(f) with gray solid lines, the same as Fig. 1(f).

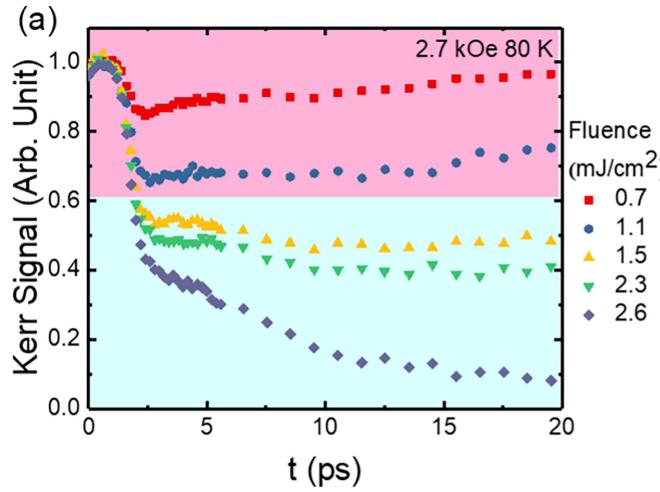

FIG. 3. Fluence dependence of the ultrafast demagnetization dynamics at an ambient temperature 80 K and external magnetic field of 2.7 kOe.

In addition to ambient temperature and applied magnetic field, laser fluence can also induce the transition from type-I to type-II demagnetization. Figure 3 presents ultrafast demagnetization curves at 80 K with varying the fluence of pump pulse F from 0.7–2.6 mJ/cm^2. A critical fluence of $F = 1.1$ mJ/cm^2 was observed to trigger the transition from type-I to type-II demagnetization. Recently, ultrafast cryo-Lorentz transmission electron microscopy demonstrated that skyrmion lattice can be manipulated during the laser-induced demagnetization [8]. For skyrmion writing process, threshold values 0.16–5.0 mJ/cm^2 are required in temperature ranging from 150 to 230 K. The same order of magnitude as the critical fluence for triggering a transition from one-step to two-step ultrafast demagnetization suggests that the slow demagnetization plays a leading role in the manipulation of skyrmions. Owing to the broader phase region of skyrmion in the epitaxial FeGe thin film, the critical laser fluence for two-step ultrafast demagnetization in our film is lower than the writing threshold in the corresponding bulk material used in Ref. [8].

C. M3TM analysis

In order to provide a microscopic insight into the origin of the transition from one-step to two-step demagnetization in FeGe film, we employed the M3TM [2] proposed by Koopmans *et al.* to fit ultrafast demagnetization curves of FeGe film. The following set of differential equations was used:

$$C_e \frac{dT_e}{dt} = g_{e-p}(T_p - T_e) + P(t), \quad (2)$$

$$C_p \frac{dT_p}{dt} = g_{e-p}(T_e - T_p), \quad (3)$$

$$\frac{dm}{dt} = Rm\frac{T_p}{T_c}\left(1 - m\coth\left(\frac{mT_c}{T_e}\right)\right), \quad (4)$$

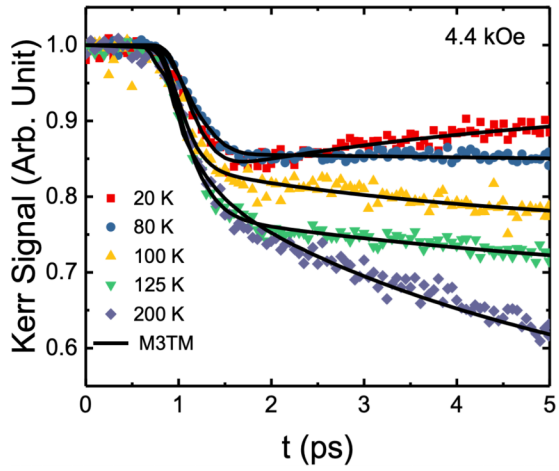

FIG. 4. M3TM fitting for the ultrafast demagnetization curves at 4.4 kOe.

where C_e and C_p are the heat capacity of electron and phonon system, respectively. g_{e-p} is the macroscopic *e-p* coupling parameter. $m = M/M_s$ (the magnetization relative to its value at zero temperature) and R is a materials-specific scaling factor for the demagnetization rate. T_e, T_p, and T_c represent the electron temperature, phonon temperature, and Curie temperature, respectively. $P(t)$ is the input laser pulse power. According to this model, we can observe that the type of demagnetization with various temperature as well as laser fluence depends strongly on the parameter of R. For materials with $R \gg 1/\tau_{e-p0}$, where τ_{e-p0} is defined as electron-phonon relaxation time τ_{e-p} at $T \approx T_c$, type-I demagnetization is shown whatever the temperature and laser fluence. For materials with $R \ll 1/\tau_{e-p0}$, the type-II demagnetization is dominant. We found that the obtained timescales by the phenomenological three-temperature model are very close to that of type I obtained by Eq. (1).

By fitting the temperature scheme as solid lines plotted in Fig. 4 with the thermal constants from Ref. [26], we yield the *e-p* coupling constant $g_{e-p} = (0.75 \pm 0.21) \times 10^{18}$ J/(sm^3 K), and the scaling factor for the demagnetization rate $R = 0.9 \pm 0.2$ ps^{-1}. The microscopic $e - p$ coupling constant $\lambda_{e-p} = 4.54 \pm 1.13$ meV was estimated using the equation

$$g_{e-p} = 3\pi D_F^2 D_p k_B^2 T_D \lambda_{e-p}^2/(2\hbar), \tag{5}$$

where $\hbar$ is the Planck constant, k_B is the Boltzmann constant, D_p is the amount of possible phonon polarization states (usually one longitudinal and two transverse), the electronic density of states at the Fermi level in a free-electron mode is $D_F = 17.8$ states/(eV unit cell), and the Debye temperature is $T_D = 370$ K [27].

Type-I demagnetization is generally expected to occur when coupling between the electron and spin system is strong, whereas type-II demagnetization is present when the electron-spin (*e-s*) coupling is weak. However, in FeGe film, we found that the microscopic *e-p* coupling constant $\lambda_{e-p} = 4.54$ meV of FeGe film is much smaller than that of Ni($\lambda_{e-p} = 26$ meV) and other ferrimagnets and ferromagnets ($\lambda_{e-p} \sim 20$ meV) [24]. Due to weak *e-p* coupling, the temperature rise of phonons lags behind that of electrons, and consequently the magnetization further decays with a larger timescale, i.e., two-step (type-II) demagnetization.

D. Transient reflectivity

To further confirm the weak *e-p* coupling obtained by the M3TM analysis, the transient reflectivity ΔR at various temperatures and magnetic fields was measured. As shown in Figs. 5(a) and 5(b), a sharp increase in the reflectivity during the pump-pulse duration, consistent with enhanced electronic occupancy above the Fermi energy, followed by a fast decrease in about 4.8 ps (electron-phonon relaxation time) and a slow relaxation up to several hundred picoseconds (thermal diffusion). With varying temperature and magnetic field, there are no obvious changes in the shape of the curves, indicating that the *e-p* coupling is not sensitive to temperature and spin orders. Compared with the transient reflection change of metals [30] and semiconductor [19], one can find that the electron-phonon relaxation time of 4.8 ps for FeGe film is significantly longer, implying a weaker *e-p* coupling.

IV. DISCUSSION

In the M3TM it is assumed that based on the Elliott-Yafet type of scattering, described by a probability $a_{\rm sf}$, that an electron flips its spin on emission or absorption of a phonon induced by spin-orbit coupling (SOC) [2]. In a material with SOC the electronic states are a mixture of a dominant spin-up (down) and a small spin-down (up) contribution. The spin-flip probability $a_{\rm sf} = 0.03 \pm 0.02$ was estimated from the fitting parameter R using the equation [2]

$$R = 8 a_{\rm sf} T_C^2 g_{e-p}/k_B T_D^2 D_s, \tag{6}$$

It is generally expected that $a_{sf} \propto Z^4$ owing to SOC, where Z is the nuclear charge. It is noteworthy that the spin-flip probability of FeGe is less than those of Ni(0.185 ± 0.015), Co(0.150 ± 0.015), and Gd (0.08 ± 0.02) [2]. Carva *et al.* observed that the spin-flip probability in Ni strongly depends on the electron energy (temperature) and a larger demagnetization is obtained for nonequilibrium electron distribution [31]. A smaller $a_{\rm sf}$ implies that there are not enough flipped spins to facilitate the magnetic configuration reconstruction at low temperatures. Because of the weak *e-p* coupling, lower Curie temperature, as well as smaller $a_{\rm sf}$, the value of R in FeGe is much smaller than that in Ni [2,32] As a result, the threshold temperature for type-II demagnetization in FeGe is about 100 K, which is far below its Curie temperature. In contrast to previous two-step ultrafast demagnetization processes in different systems, i.e., ferromagnetic transition metals, rare-earth metals [33,34], half-metallic magnetic oxides [35–37], and Heusler alloy [38,39], our results show that the transition undergoes in a broader temperature range far from Curie temperature.

Although the model can explain that the two-step demagnetization is caused by the weak *e-p* coupling, the variation of demagnetization time related to the magnetic field/phase cannot give a reasonable explanation because M3TM is not associated with noncollinear magnetic structures. The demagnetization times are strongly related to the magnetic phase and there is a clear transition from type I to type II at 100 K. In chiral magnets, the different spin texture

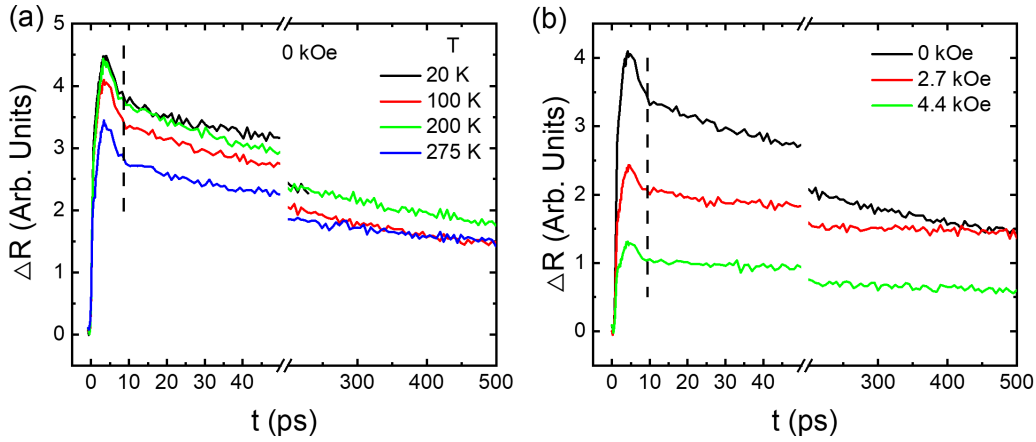

FIG. 5. Time dependence of the laser-induced transient reflectivity (a) at 20, 100, 200, and 275 K with 0-kOe magnetic field and (b) at 100 K with 0-, 2.7-, and 4.4-kOe magnetic fields.

results from the competition between exchange interaction, DMI, magnetocrystalline anisotropy, and Zeeman interaction. Thus, demagnetization in principle should also be affected by the combination of these factors. Based on understanding of electron-spin (*e-s*) scattering, we can assume that the enhancement of electron-spin scattering occurs when the magnetic configuration changes from a collinear (parallel) to a noncollinear configuration. Therefore, we can expect longer demagnetization times as the spins go from collinear to noncollinear. It should be mentioned that the *e-s* scattering is not included in the M3TM model, and consequently leads the presence of an additional spin-flip mechanism in the noncollinear phase. One should be noted that in the chiral magnet FeGe, the longest demagnetization time does not occur at the smallest magnetic field, which may be caused by the topology of the skyrmions.

V. SUMMARY

In summary, the ultrafast demagnetization behavior of chiral magnet FeGe film has been investigated using pump-probe time-resolved magneto-optical Kerr effect. A transition from one-step to two-step demagnetizations with varying ambient temperature, magnetic field, as well as laser fluence was observed. In the region of skyrmion phase, TRMOKE curves demonstrate a two-step ultrafast demagnetization process. Our work can provide more information for the ultrafast spin dynamics of nonlinear magnetic structure and open an avenue to explore chiral magnetic devices on picosecond timescales.

ACKNOWLEDGMENTS

This work is supported by the National Key R&D Program of China (Grant No. 2022YFA1403302), and the National Natural Science Foundation of China (Grants No. 11874411, No. 52031015, and No. U22A20115). W.Z. gratefully acknowledges the National Natural Science Foundation of China (Grant No. 12104030) and China Postdoctoral Science Foundation (Grant No. 2022M710320).

[1] A. Kirilyuk, A. V. Kimel, and T. Rasing, Ultrafast optical manipulation of magnetic order, Rev. Mod. Phys. **82**, 2731 (2010).

[2] B. Koopmans, G. Malinowski, F. Dalla Longa, D. Steiauf, M. Fahnle, T. Roth, M. Cinchetti, and M. Aeschlimann, Explaining the paradoxical diversity of ultrafast laser-induced demagnetization, Nat. Mater. **9**, 259 (2010).

[3] O. Matsuda, M. C. Larciprete, R. Li Voti, and O. B. Wright, Fundamentals of picosecond laser ultrasonics, Ultrasonics **56**, 3 (2015).

[4] B. Pfau, S. Schaffert, L. Muüller, C. Gutt, A. Al-Shemmary, F. Buüttner, R. Delaunay, S. Duüsterer, S. Flewett, R. Froümter *et al.*, Ultrafast optical demagnetization manipulates nanoscale spin structure in domain walls, Nat. Commun. **3**, 1100 (2012).

[5] F. Buüttner, B. Pfau, M. Boüttcher, M. Schneider, G. Mercurio, C. M. Guünther, P. Hessing, C. Klose, A. Wittmann, K. Gerlinger *et al.*, Observation of fluctuation-mediated picosecond nucleation of a topological phase, Nat. Mater. **20**, 30 (2021).

[6] N. Nagaosa and Y. Tokura, Topological properties and dynamics of magnetic skyrmions, Nat. Nanotechnol. **8**, 899 (2013).

[7] Y. Xu, M. Deb, G. Malinowski, M. Hehn, W. Zhao, and S. Mangin, Ultrafast magnetization manipulation using single femtosecond light and hot-electron pulses, Adv. Mater. **29**, 1703474 (2017).

[8] G. Berruto, I. Madan, Y. Murooka, G. M. Vanacore, E. Pomarico, J. Rajeswari, R. Lamb, P. Huang, A. J. Kruchkov, Y. Togawa *et al.*, Laser-Induced Skyrmion Writing and Erasing in an Ultrafast Cryo-Lorentz Transmission Electron Microscope, Phys. Rev. Lett. **120**, 117201 (2018).

[9] N. Ogawa, S. Seki, and Y. Tokura, Ultrafast optical excitation of magnetic skyrmions, Sci. Rep. **5**, 9552 (2015).

[10] S. G. Je, P. Vallobra, T. Srivastava, J. C. Rojas-Sanchez, T. H. Pham, M. Hehn, G. Malinowski, C. Baraduc, S. Auffret, G. Gaudin *et al.*, Creation of magnetic skyrmion bubble lattices by ultrafast laser in ultrathin films, Nano Lett. **18**, 7362 (2018).

[11] C. D. Stanciu, F. Hansteen, A. V. Kimel, A. Kirilyuk, A. Tsukamoto, A. Itoh, and T. Rasing, All-Optical Magnetic Recording with Circularly Polarized Light, Phys. Rev. Lett. **99**, 047601 (2007).

[12] J. Walowski and M. Munzenberg, Perspective: Ultrafast magnetism and THz spintronics, J. Appl. Phys. **120**, 140901 (2016).

[13] B. Lenk, H. Ulrichs, F. Garbs, and M. Munzenberg, The building blocks of magnonics, Phys. Rep. **507**, 107 (2011).

[14] S. Muhlbauer, B. Binz, F. Jonietz, C. Pfleiderer, A. Rosch, A. Neubauer, R. Georgii, and P. Boni, Skyrmion lattice in a chiral magnet, Science **323**, 915 (2009).

[15] X. Z. Yu, N. Kanazawa, Y. Onose, K. Kimoto, W. Z. Zhang, S. Ishiwata, Y. Matsui, and Y. Tokura, Near room-temperature formation of a skyrmion crystal in thin-films of the helimagnet FeGe, Nat. Mater. **10**, 106 (2011).

[16] W. Münzer, A. Neubauer, T. Adams, S. Mühlbauer, C. Franz, F. Jonietz, R. Georgii, P. Böni, B. Pedersen, M. Schmidt *et al.*, Skyrmion lattice in the doped semiconductor $Fe_{1-x}Co_xSi$, Phys. Rev. B **81**, 041203(R) (2010).

[17] J. Gayles, F. Freimuth, T. Schena, G. Lani, P. Mavropoulos, R. A. Duine, S. Blugel, J. Sinova, and Y. Mokrousov, Dzyaloshinskii-Moriya Interaction and Hall Effects in the Skyrmion Phase of $Mn_{1-x}Fe_xGe$, Phys. Rev. Lett. **115**, 036602 (2015).

[18] S. V. Grigoriev, N. M. Potapova, S. A. Siegfried, V. A. Dyadkin, E. V. Moskvin, V. Dmitriev, D. Menzel, C. D. Dewhurst, D. Chernyshov, R. A. Sadykov *et al.*, Chiral Properties of Structure and Magnetism in $Mn_{1-x}Fe_xGe$ Compounds: When the Left and the Right Are Fighting, Who Wins?, Phys. Rev. Lett. **110**, 207201 (2013).

[19] J. D. Koralek, D. Meier, J. P. Hinton, A. Bauer, S. A. Parameswaran, A. Vishwanath, R. Ramesh, R. W. Schoenlein, C. Pfleiderer, and J. Orenstein, Observation of Coherent Helimagnons and Gilbert Damping in an Itinerant Magnet, Phys. Rev. Lett. **109**, 247204 (2012).

[20] Z. Chen and L. W. Wang, Role of initial magnetic disorder: A time-dependent ab initio study of ultrafast demagnetization mechanisms, Sci. Adv. **5**, eaau8000 (2019).

[21] F. Zheng, F. N. Rybakov, A. B. Borisov, D. Song, S. Wang, Z.-A. Li, H. Du, N. S. Kiselev, J. Caron, A. Kovács *et al.*, Experimental observation of chiral magnetic bobbers in B20-type FeGe, Nat. Nanotechnol. **13**, 451 (2018).

[22] J. Tang, Y. D. Wu, W. W. Wang, L. Y. Kong, B. Y. Lv, W. S. Wei, J. D. Zang, M. L. Tian, and H. F. Du, Magnetic skyrmion bundles and their current-driven dynamics, Nat. Nanotechnol. **16**, 1086 (2021).

[23] S. X. Huang and C. L. Chien, Extended Skyrmion Phase in Epitaxial FeGe(111) Thin Films, Phys. Rev. Lett. **108**, 267201 (2012).

[24] T. Roth, A. J. Schellekens, S. Alebrand, O. Schmitt, D. Steil, B. Koopmans, M. Cinchetti, and M. Aeschlimann, Temperature Dependence of Laser-Induced Demagnetization in Ni: A Key for Identifying the Underlying Mechanism, Phys. Rev. X **2**, 021006 (2012).

[25] A. S. Ahmed, J. Rowland, B. D. Esser, S. R. Dunsiger, D. W. McComb, M. Randeria, and R. K. Kawakami, Chiral bobbers and skyrmions in epitaxial FeGe/Si(111) films, Phys. Rev. Mater. **2**, 041401(R) (2018).

[26] H. Yamada, K. Terao, H. Ohta, and E. Kulatov, Electronic structure and magnetism of FeGe with B20-type structure, Physica B **329**, 1131 (2003).

[27] H. Wilhelm, A. O. Leonov, U. K. Rossler, P. Burger, F. Hardy, C. Meingast, M. E. Gruner, W. Schnelle, M. Schmidt, and M. Baenitz, Scaling study and thermodynamic properties of the cubic helimagnet FeGe, Phys. Rev. B **94**, 144424 (2016).

[28] A. Bauer and C. Pfleiderer, Magnetic phase diagram of MnSi inferred from magnetization and ac susceptibility, Phys. Rev. B **85**, 214418 (2012).

[29] J. C. Gallagher, K. Y. Meng, J. T. Brangham, H. L. Wang, B. D. Esser, D. W. McComb, and F. Y. Yang, Robust Zero-Field Skyrmion Formation in FeGe Epitaxial Thin Films, Phys. Rev. Lett. **118**, 027201 (2017).

[30] R. W. Schoenlein, W. Z. Lin, J. G. Fujimoto, and G. L. Eesley, Femtosecond Studies of Nonequilibrium Electronic Processes in Metals, Phys. Rev. Lett. **58**, 1680 (1987).

[31] K. Carva, M. Battiato, and P. M. Oppeneer, Ab Initio Investigation of the Elliott-Yafet Electron-Phonon Mechanism in Laser-Induced Ultrafast Demagnetization, Phys. Rev. Lett. **107**, 207201 (2011).

[32] E. Beaurepaire, J. Merle, A. Daunois, and J. Bigot, Ultrafast Spin Dynamics in Ferromagnetic Nickel, Phys. Rev. Lett. **76**, 4250 (1996).

[33] M. Wietstruk, A. Melnikov, C. Stamm, T. Kachel, N. Pontius, M. Sultan, C. Gahl, M. Weinelt, H. A. Durr, and U. Bovensiepen, Hot-electron-driven Enhancement of Spin-Lattice Coupling in Gd and Tb 4f Ferromagnets Observed by Femtosecond X-Ray Magnetic Circular Dichroism, Phys. Rev. Lett. **106**, 127401 (2011).

[34] A. Mekonnen, A. R. Khorsand, M. Cormier, A. V. Kimel, A. Kirilyuk, A. Hrabec, L. Ranno, A. Tsukamoto, A. Itoh, and T. Rasing, Role of the inter-sublattice exchange coupling in short-laser-pulse-induced demagnetization dynamics of GdCo and GdCoFe alloys, Phys. Rev. B **87**, 180406(R) (2013).

[35] Q. Zhang, A. V. Nurmikko, A. Anguelouch, G. Xiao, and A. Gupta, Coherent Magnetization Rotation and Phase Control by Ultrashort Optical Pulses in CrO(2) Thin Films, Phys. Rev. Lett. **89**, 177402 (2002).

[36] T. Ogasawara, K. Ohgushi, Y. Tomioka, K. S. Takahashi, H. Okamoto, M. Kawasaki, and Y. Tokura, General Features of Photoinduced Spin Dynamics in Ferromagnetic and Ferrimagnetic Compounds, Phys. Rev. Lett. **94**, 087202 (2005).

[37] T. Kise, T. Ogasawara, M. Ashida, Y. Tomioka, Y. Tokura, and M. Kuwata-Gonokami, Ultrafast Spin Dynamics and Critical Behavior in Half-Metallic Ferromagnet: Sr_2FeMoO_6, Phys. Rev. Lett. **85**, 1986 (2000).

[38] A. Mann, J. Walowski, M. Munzenberg, S. Maat, M. J. Carey, J. R. Childress, C. Mewes, D. Ebke, V. Drewello, G. Reiss *et al.*, Insights into Ultrafast Demagnetization in Pseudogap Half-Metals, Phys. Rev. X **2**, 041008 (2012).

[39] A. Bonda, S. Uba, and L. Uba, Laser-induced two-step demagnetization process study in Ni–Mn–Sn Heusler alloy film, J. Magn. Magn. Mater. **546**, 168805 (2022).